Yong-gang LI 论文集

抽印本(Reprinted from)

地 学 前 缘
EARTH SCIENCE FRONTIERS

ONE OF THE MOST IMPORTANT JOURNALS OF EARTH SCIENCE
IN CHINA AND EACH ISSUE WITH A SPECIAL TOPIC

地学前缘 2003 年 第 10 卷 第 4 期
Earth Science Frontiers 2003 Vol 10 No 4

CHARACTERIZATION OF RUPTURE ZONES AT LANDERS AND HECTOR MINE, CALIFORNIA IN 4-D BY FAULT-ZONE GUIDED WAVES

Yong-gang LI

(*Department of Earth Sciences, University of Southern California, Los Angeles, California* 90089, *U. S. A.*)

中国地质大学(北京)
China University of Geosciences(Beijing)

CHARACTERIZATION OF RUPTURE ZONES AT LANDERS AND HECTOR MINE, CALIFORNIA IN 4-D BY FAULT-ZONE GUIDED WAVES

Yong-gang LI

(*Department of Earth Sciences, University of Southern California, Los Angeles, California* 90089, *U. S. A.*)

断层导波研究加利福尼亚兰德斯和海克特曼恩地震断层带的四维特征

摘　要:美国加利福尼亚州兰德斯和海克特曼恩地区于1992年和1999年先后发生7.4级和7.1级地震,分别在地面产生80 km和40 km长的断裂带。震后在断裂带布置的密集地震站台记录到明显的断层导波(fault-zone guided waves)。这些导波由断层带内的余震和人工震源激发产生,走时在S波之后,但具有比体波更强的振幅和更长的波列,并具有频散特征。通过对2~7 Hz断层导波的定量分析和三维有限差分数字模拟,获得了震深区断裂带的高分辨内部构造图像以及岩石的物理特性。数字模拟结果表明这些断裂带上存在被严重破碎了的核心层,形成低速、低Q值地震波导。核心破碎带宽约100~200 m,其内地震波波速降为周围岩石的40%~50%,Q值约为10~50。根据岩石断裂力学观点,这一低速、低Q值带可被解释为地震过程中处于断层动态断裂前端的非弹性区(或称之为破碎区,相干过程区)。在兰德斯和海克特曼恩断裂带测得的破碎区宽度与断裂带长度之比约为0.005,基本上符合岩石断裂力学预期的结果。观察到的断层导波还显示兰德斯和海克特曼恩地震中多条断层发生滑移和破碎。兰德斯地震时多条阶梯形断层相继断裂;而在海克特曼恩地震中,断裂带南北两端均出现分枝断裂,深处的分枝断裂较地表出现的破裂状况更为复杂。由三维有限元模拟的动态断裂过程表明,海克特曼恩地震中出现的分枝断裂现象极有可能发生,并与断层导波解析出的波导分叉结果相吻合。震后在兰德斯断裂带使用人工爆炸震源测量地震波速度变化的重复实验显示断裂带内S波波速于1994至1996年两年内增快了约1.2%,随后于1996至1998年两年内又提高了约0.7%。但在断裂带外,波速随时间的变化并不明显。从而说明兰德斯断裂带内由1992年7.4级地震产生的大量岩石裂隙很可能在主震后逐渐愈合,岩石强度逐渐恢复。计算结果表明1994年至1998年4年间兰德斯断裂带内S波波速增快了约2.0%,相当于岩石孔隙视密度减少了约0.03,或岩石剪切模量提高了约1%。重复实验结果同时显示在这4年间隔内P波和S波走时变化之比由0.75降为0.65,说明断裂带内岩石孔隙水含量在1992年震后又逐渐增加。在海克特曼恩断裂带使用人工爆炸震源的重复性实验进而显示震后断层愈合这一普遍现象。数据表明断裂带内S波波速于2000年和2001年1年内增快了0.65%~1.0%,表明断层愈合速率并非常量,在震后初期愈合得较快,同时各段断层愈合快慢也不一致。主震中位移较大、岩石破碎较严重的断层主震后愈合率较大。我们还发现兰德斯断裂带的愈合过程在1999年受到了邻近发生的7.1级海克特曼恩地震的影响。这一强震产生的应力波和大地形变造成兰德斯断裂带内原本脆弱的岩石相应破裂,产生了附加的孔隙视密度,因此,1998年和2000年在兰德斯断裂带测得的数据显示S波波速反而降低了约0.5%。经过这一逆变化后,兰德斯断层愈合过程又恢复了正常。使用地震断层导波对加州兰德斯和海克特曼恩断裂带所做的四维研究,使我们进一步认识和了解地震断层带的内部精细结构和岩石物理特性,以及活动断层上普遍存在的断裂—愈合—再断裂的地震周期性,取得这些结果对今后评估和预测地震具有指导意义。

关键词:断层;导波;四维;地震;兰德斯断裂带;海克特矿;加利福尼亚

中图分类号:P315.3　**文献标识码**:A　**文章编号**:1005-2321(2003)04-0479-27

收稿日期:2003-03-09;**修订日期**:2003-09-08

基金项目:美国国家科学基金项目(EAR 9104762, EAR-9801811, EAR-0105508)

作者简介:Yong-gang LI,男,美国南加州大学地球科学系教授。E-mail:ygli@terra.usc.edu

0 Introduction

The fine structure of fault zones is of great interest because the factors that control the initiation, propagation, and termination of rupture are not well understood yet. Observations suggest that fault zone complexity may segment fault zones [*Aki*, 1984; *Malin et al.*, 1989; *Ellsworth*, 1990; *Beck and Christensen*, 1991] or control the timing of moment release in earthquakes [*Harris and Day*, 1993; *Wald and Heaton*, 1994]. Rupture models have been proposed that involved variations in pore-fluid pressure over the earthquake cycle [*Hickman et al.*, 1995; *Blanpied et al.*, 1998]. Other studies predict that most earthquake energy is stored in areas with less developed fault zones [*Mooney and Ginzburg*, 1986] or with higher velocity rock outside the fault [*Michelini and McEvilly*, 1991]. Geometrical, structural, and rheological fault discontinuities, caused by the spatial variations in strength and stress will affect the earthquake rupture [e. g., *Wesson and Ellsworth*, 1973; *Das and Aki*, 1977; *Rice*, 1980; *Day*, 1984]. Rupture segmentation is often related to fault bends, step-overs, branches, and terminations that have been recognized by surface mapping [e. g., *Sieh et al.*, 1993; *Johnson et al.*, 1997], exhumation [e. g., *Chester et al.*, 1993], and seismic profiling and tomography [e. g., *Lees and Malin*, 1990; *Thurber et al.*, 1997].

Because the fault plane is thought to be a weakness plane in the earth crust, it facilitates slip to occur under the prevailing stress orientation. As suggested by laboratory experiments, shear faulting is highly resisted in brittle rock and proceeds as re-activated faults along surfaces which have already encountered considerable damage. Field evidence shows that the rupture plane of slip on a mature fault occurs at a more restricted position, the edge of damage zone at the plane of contact with the intact wall rock. Assuming that this is an actual picture of rupture preparation on the major faults, defining the fine internal structure of active fault zones is a challenging problem to seismologists and geologists.

Structurally, major crustal faults are often marked by zones of lowered velocity with a width of a few hundred meters to a few km [e. g. *Michelini and McEvilly*, 1991; *Li et al.*, 2000]. These low-velocity zones are thought to be caused by intense fracturing during earthquakes, brecciation, liquid-saturation and possibly high pore-fluid pressure near the fault [*Nur*, 1972; *Sibson*, 1977]. The strength of the low-velocity anomalies in fault-zone rocks might vary over the earthquake cycle [*Vidale et al.*, 1994; *Marone*, 1998; *Li et al.*, 1998a]. As a result of the seismic velocity reduction, the fault zone forms a natural low-velocity waveguide to trap and focus seismic energy as normal modes when a source located in or close to the fault zone.

Since fault zone trapped waves were discovered on active faults at Oroville and Parkfield, California, these waves have enabled us to evaluate the internal structure and material properties of fault zones at seismogenic depths with a higher resolution than ever before [*Li et al.*, 1990]. Because fault zone trapped waves arise from coherent multiple reflections at the boundaries between the low-velocity fault zone and the high-velocity surrounding rock, the amplitudes, frequencies and dispersive waveforms of trapped modes strongly depend on the fault geometry and physical properties [*Li and Leary*, 1990; *Li and Vidale*, 1996; *Ben-Zion*, 1998]. Observations and numerical modeling of fault-zone trapped waves at the San Andreas fault, San Jacinto fault and rupture zones of the 1992 *M*7.4 Landers and 1999 *M*7.1 Hector Mine earthquakes in California and the 1995 *M*6.9 Kobe earthquake in Japan, have documented a detailed internal structure and physical properties of fault zones at seismogenic depths [*Li et al.*, 1994a, b; *Li et al.*, 1997a, b; *Li et al.*, 1998b]. These active faults are marked by a low-velocity zone about tens to a few hundred meters wide where the shear velocity is reduced by 30%~50% from the wall-rock velocities and Q is about 10~60. From the point view of fracture mechanics [e. g., *Rice*, 1980; *Papageorgiou and Aki*, 1983; *Scholz*, 1990], we interpreted the low-velocity waveguide inferred by fault-zone trapped waves as a remanent of damage zone (break-down zone, process zone) in crustal rock during dynamic rupture in the recent major earthquakes while it probably also represents the accumulated wear zone from many historical earthquakes on them.

This paper illuminates the high resolution delineation of rupture zones of the 1992 *M*7.4 Landers and 1999 *M*7.1 Hector Mine earthquakes in 3-D using fault-zone trapped waves, and shows the post-seismic fault healing (strength recovery with time) on the rupture zones. It concentrates on the fault segmentation, depth-dependent damage degree and extent of fault zone to adjacent rocks as well as fault-zone rock rigidity and strength recovery with time. The knowledge of spatial and temporal (4-D) patterns in fault zone structure and material properties will help predict the behavior of future earthquakes on active faults, and will also help evaluate the fault rupture models as well.

1 At the Landers Rupture Zone

The *M*7.4 Landers earthquake on June 26, 1992 produced surface breaks of total 70 km in the length with the maximum right-lateral slip of 7 m in Mojave desert, California (Fig. 1a). Immediately after the mainshock, a mobile seismic array of 9 three-component seismometers was used at 11 sites along the rupture zone from the Johnson Valley fault (JVF) to Camp Rock fault (CRF) to acquire fault-zone trapped waves generated by aftershocks [*Li et al.*, 1994a]. Prominent trapped waves at 3~6 Hz with large amplitudes and long duration were recorded within the rupture zone. Two months later, we installed denser seismic arrays composed by 31 three-component stations operated by the personal computer (PC) recording system of the US Geological Survey and 15 PASSCAL's REFTEK seismometers of IRIS (Center of Incorporated Institutions for Seismology) at a site (Line 1 in Fig. 1b) on the JVF to record extensive data. About 250 aftershocks were recorded in 5 days. These data have been used to characterize the internal structure and segmentation of the Landers rupture [*Li et al.*, 1994a, b]. We also detonated near-surface explosions within the rupture zone in repeated seismic surveys starting from 1994 to monitor the temporal variations in the zone. In repeated experiments, 73 REFTEK seismometers were deployed at the same locations on Lines 1, 2, and 3 across and along the JVF (Lander southern rupture segment), and 3 explosions were detonated at the same places within the fault zone(Fig. 1b).

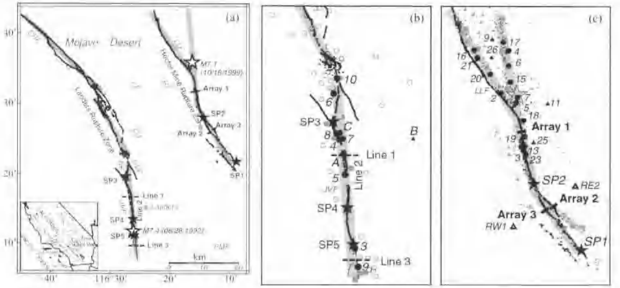

Fig. 1 (a) Map shows locations of seismic arrays deployed at rupture zones of the 1992 *M*7.4 Landers and the 1999 *M*7.1 Hector Mine, California, earthquakes, seismic arrays, and explosions. Shaded zones show rupture zones inferred from seismic and geodetic studies. BF, Bullion fault; CF, Calico fault; CRF, Camp Rock fault; ELF, Emerson Lake fault; JVF, Johnson Valley fault; KF, Kickapoo fault; HVF, Homestead Valley fault; and PMF, Pinto Mountain fault. (b) Map of Landers area shows locations of arrays deployed on 3 seismic lines across and along the Johnson Valley fault, 3 shots detonated within the rupture zone, and aftershocks recorded during experiments. Grey circles denote aftershocks showing prominent fault-zone trapped waves while open circles denote events without clear trapped waves. Black circles and triangles with labels and numbers are aftershocks which waveform data used in this paper to show with and without fault-zone guided waves. (c) As the same in (a) but for Hector Mine area. Grey circles and triangles denote aftershocks generating prominent fault-zone guided waves or not. RW1 and RE2 were remote stations deployed away from the rupture zone

图1 (a)图示加利福尼亚兰德斯(1992年M7.4)和海克特曼恩(1999年M7.1)地震震中及在断裂带布置的地震台阵及人工爆炸震源位置;(b)兰德斯地震带内横跨和沿着Johuson Valley断层(JVF)布置的3条地震测线及部分余震及人工爆炸震源位置图;(c)海克特曼恩地震带内横跨Lavic Lake断层(LLF)布置的3条地震测线及部分余震及爆炸震源位置图

The explosion exciting trapped waves were first combined with those generated by aftershocks to document the depth dependent structure of the rupture zone [*Li et al*. 1999, 2000]. With the added iterations, these data were used for probing the fault healing with time.

For example, Fig. 2a exhibits seismograms recorded at the cross-fault array on Line 1 for 3 aftershocks (events A, B, and C in Fig. 1b) occurring at depths of 4~10 km within and out of the Landers

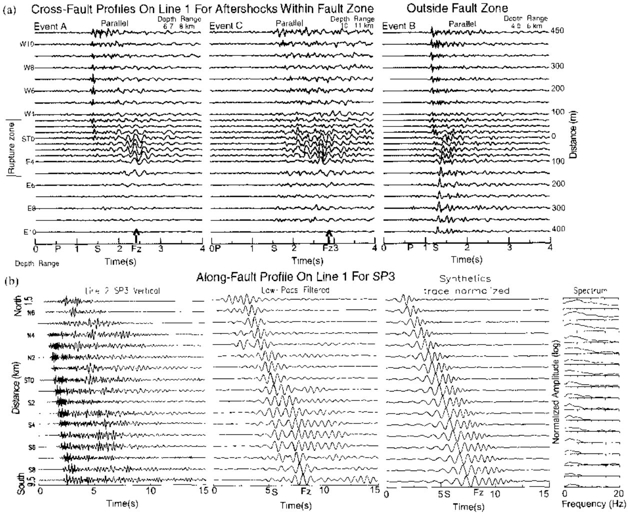

Fig. 2 (a) Parallel-fault component seismograms recorded at Line 1 across the JVF for 3 aftershocks (Events A, B, and C in Fig. 1b). Station ST0 of the array was located on the main fault trace. Station names beginning with E or W denote the station located east or west of the fault trace. Station spacings are not even, 25 m for stations close to the fault and 50~100 m for farther stations. Depths and hypocentral distances (range in km) of aftershocks are plotted for each event. Vertical grey lines align with S wave arrivals. Fault-zone trapped waves (Fz) are prominent (denoted by red arrows) at stations located near the surface fault trace for events A and C occurring within the rupture zone but not for event B far away from the rupture zone. Solid bars mark the rupture zone width in which fault zone trapped waves are dominant. (b) Vertical component seismograms recorded at Line 2 along the JVF for shot SP3 detonated within the rupture zone at 1.5 km north of the array. Station spacing was 500 m. seismograms are plotted in trace normalized profile. Trapped waves are clear in low-pass (<3 Hz) filtered seismograms. Grey lines align with arrivals of P, S and dominant trapped waves. Synthetic fault-zone guided waves using model parameters in Fig. 4b are comparable to observations. Coda-normalized amplitude spectra of seismograms are plotted using a logarithmic scale, from which Q values of fault-zone rocks could be estimated

图 2 (a)由横跨 JVF 的测线 1 记录到的由 3 个兰德斯余震(图 1b 中地震序号 A,B 和 C)产生的平行断层分量上的地震波形图;(b)沿着 JVF 的测线 2 上记录到的由爆炸震源 SP3 产生的垂直分量波形图和振幅频率谱。震源 SP3 位于测线 2 北端 1.5 km 处

rupture zone, respectively. The array was 850 m long and included 22 three-component stations with uneven station spacing of 25 and 50 m. Trapped waves with large amplitudes and long-duration wavetrains at 3～5 Hz following S waves appeared at stations between W2 and E6 located close to the main fault trace for events A and C occurring on the JVF, but not for event B occurring ～5 km away from the fault zone. Stations located out of the rupture zone registered a brief S wave, without significant trapped waves for 3 events. These observations show the existence of a low-velocity waveguide on the JVF to trap and focus seismic energy within it. Based on the distance between stations W2 and E6 in which trapped waves were prominent, we estimated the width of the low velocity rupture zone on the JVL to be 250 m at surface, consistent with the width of the shear zone spanning all surface breaks in rupture zone on both sides of the main fault trace mapped by *Johnson et al.* [1997] after the Landers earthquake. It is noted that the rupture zone is not symmetry with the main fault trace that is located closer to the west edge of the rupture zone.

Fig. 2b illustrates seismograms recorded at Line 2 along the JVF for a near surface explosion SP3 located within the rupture zone. Line 2 was 8 km long and consisted of 16 3-channel REFTEK recorders with the station spacing of 500 m. SP3 used 400 kg chemical explosives in a 40 m deep shot-hole drilled within the rupture zone 1.5 km north of Line 2. Explosion-exciting trapped waves show large amplitude and long-duration wavetrains following S waves, similar to those generated by aftershocks but at lower frequencies (1～3 Hz), indicating that the waveguide on the shallower part of the JVF is slower and probably wider than the deep part of the fault zone. The separation between the S waves and dominant trapped waves increases nearly constantly with distance between the shot and station, as expected for trapped waves traveling along a continuous rupture zone with slower velocities than surrounding rocks. Trapped waves at lower frequencies travel faster than at higher frequencies, showing dispersion of trapped waves. The spectral amplitudes of trapped waves were also computed and normalized by coda waves. We computed amplitude spectra of fault-zone guided waves in a 5 s time windows following S arrivals and divided them by the coda wave spectra in a time window with the same length to reduce the source and receiver site affects [*Li et al.*, 1999]. The coda-normalized spectra of guided waves show a decrease in amplitude with distance along the rupture zone (Fig. 2b). from which the Q value of fault-zone rock was measured to be ～20 at 2～3 Hz within the shallow Landers rupture zone.

In order to measure the group velocities of fault-zone guided waves, we used multiple band-pass filtering technique. Fig. 3a illustrates group velocities of guided waves derived from seismograms recorded at the along-fault Line 2 for shot SP3. The measured group velocities are well agreeable with synthetic

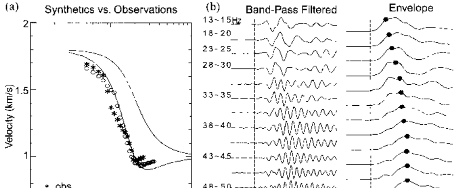

Fig. 3 (a) Computed dispersion curves for fault-zone guided waves using 2-D and 3-D model parameters given in Fig. 4b. Stars are measured group velocities on Line 2 along the Landers rupture zone for shot SP3. (b) Multiple band-pass filtered fault-parallel component seismograms and computed envelopes at station ST0 of Line 1 for an aftershock (event 8 in Fig. 1b and Fig. 4) are plotted using trace normalized scale. The guided waves at lower frequency travel faster than those at higher frequency, showing dispersion of guided waves

图3 (a)采用图1b给出的模型参数计算的二维和三维断层导向波的频散曲线和观察数据测出的导向波群速度相对照；(b)对测线1上站台ST0记录到的余震(图1b中地震序号8)波形，作多带通滤波后的平行断层分量的波行图；计算出的震幅包络线显示导波的波散特征

dispersion curves of trapped waves in terms of a fault-zone waveguide model that will be discussed later for details. The dispersion of trapped waves is shown clearly in the multiple band-pass filtered seismograms. For example, Fig. 3b exhibits seismograms at station ST0 of Line 1 located within the fault zone for an aftershock (event A in Fig. 1b). Seismograms have been filtered in 12 frequency bands between 1.3 and 5.5 Hz. Fault-zone trapped waves at lower frequencies travel faster than those at higher frequencies. Trapped waves at 4～5 Hz travel most slowly and show peak amplitudes. Because of this dispersion and concentration of fault-zone trapped waves within the low-velocity waveguide, these waves can be used to document the internal fine structure and rock physical properties in the fault zone.

Fig. 4a shows group velocities of fault-zone guided waves from multiple band-pass filtered seismograms for 3 explosions and 7 aftershocks (Fig. 1b) located at different depths within the Landers rupture zone [*Li et al.*, 2000]. The measured group velocities range from 1.9 km/s at 4 Hz to 2.6 km/s at 1 Hz for shallow events, but range from 2.3 km/s at 4 Hz to 3.1 km/s at 1 Hz for deep events, showing the depth dependent velocity structure within the rupture zone. A depth-dependent fault zone structure is expected because the increasing pressure with increasing depth will strongly affect the crack density, fluid pressure, and amount of fluids in the fault-zone rock, as well as the rate of healing of rock damage caused by earthquakes [*Sibson*, 1977; *Byerlee*, 1990]. It may also influence the development of fault gouge [*Scholz*, 1990; *Marone*, 1998]. For all these reasons, a realistic fault zone in crust is not uniform with depth.

Fault zone velocity can be estimated by considering the time lag of the fault-zone trapped waves behind the S wave. Fault zone width comes from the frequency content and dispersion of the trapped waves, and *Q* comes from the amplitude of trapped waves versus distance. Based on the measured group velocities, *Q* values and the width of the low-velocity zone inferred by trapped waves, we have constructed a depth-dependent structural model for the Landers southern rupture segment on the JVF (Fig. 4b). This model is derived by estimating the top 1～2 km of fault zone structure with profiles from explosions first. Then, the deeper structure is estimated by modeling the arrival time, amplitude, and dispersion of trapped waves from aftershocks. Combined with the results from trapped waves generated by explosions and aftershocks, Landers rupture zone is characterized by the depth-variable structure. In this structural model, the rupture zone is marked by a low velocity and low *Q* waveguide, 250 m wide at the surface and tapering to 100 m at the 10 km depth, in which shear velocities of fault-zone rock are reduced by 40%～50% from wallrock velocities and *Q* of 20～60. For example, we computed synthetic seismograms and dispersion curves of fault zone guided waves using the phase-shift technique based on propagator-matrix method [*Li and Leary*, 1990] and Green's function for Love-type waves [*Aki and Richards*, 1980] in terms of the best-fit model parameters given in Fig. 4b for the along-fault array on Line 2 and shot SP3. The synthetics matched observed trapped waveforms and group velocities quite well (see Fig. 2b and Fig. 3a). Fig. 4c shows 3-D finite difference synthetic seismograms at the cross-fault array on Line 1 for six aftershocks (events 5 to 10 in Fig. 1b) occurring within the Landers rupture zone at different depths and hypocentral distances. The 3-D finite-difference code is second order in time and fourth order in space [*Vidale*, 1989; *Graves*, 1996]. It propagates the complete wavefield through elastic media with a free surface boundary and spatially variable anelastic damping. The details in a trial-and-error forward modeling procedure for simulations of Landers fault-zone trapped waves have been discussed by *Li et al.* [2000]. The synthetic 3-D FD seismograms in Fig. 4c fit observations very well, showing that the depth dependent structural model in Fig. 4b is applicable to the Landers rupture zone. Although the model parameters obtained from a forward modeling of trapped waves are not unique because there is a trade off among them [e.g. *Li and Vidale*, 1996], the error in parameters can be reduced when independent measurements of group velocities and *Q* values are used as constraints.

Locations of aftershocks for which prominent fault zone trapped waves have been recorded at the Landers rupture zone showed the existence of low-velocity waveguides on the Landers faults. They also delineated the discontinuity between rupture segments. For instance, the guided wave inferred waveguides are disconnected at a fault stepover between the JVF and HVF (Fig. 1b), where the slip in the Landers earthquake was minimum and rupture velocity was reduced in the mainshock [*Walder and Heaton*, 1994]. This discontinuity is probably due to transient fluid pressure reductions in rocks at the dilational stepover that could arrest the rupture [*Sibson*, 1985; *Harris and Day*, 1993]. The Landers rupture appears to be a combination of rapid rupture on planar fault surface along the JVF and hesitation at fault irregularity between the JVF and the HVF. This complex in rupture process is consistent with the fault segmentation delineated by fault-zone guided waves acquired at Landers faults [*Li et al.*,

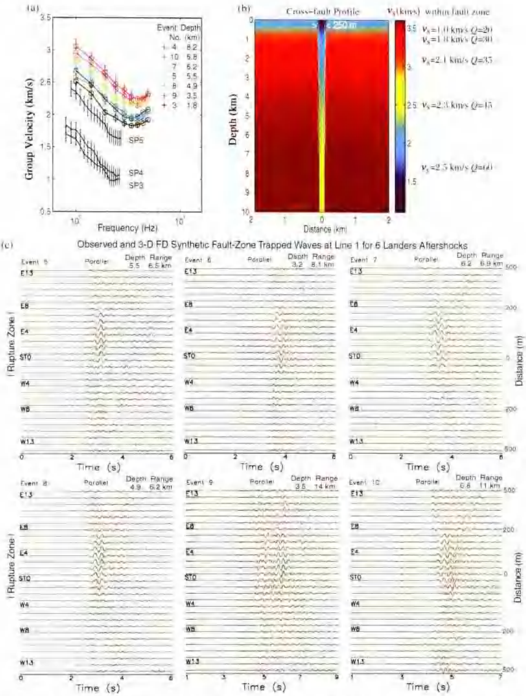

Fig. 1 (a) Group velocities of fault zone guided waves measured from multiple band-pass filtered seismograms for 3 shots and 7 aftershocks (black circles in Fig. 1b) at different depths and hypocentral distances, indicating depth-dependent velocity structure within the Landers rupture zone. Circles are the mean values of measurements at 5 stations located within the rupture zone; error bars are standard deviations. (b) The depth section of rupture zone structure model across the Johnson Valley fault. Velocities in the rupture zone are reduced by 45%~35% from wall-rock velocities. (c) 3-D finite-difference synthetic seismograms (green lines) at Line 1 for six Landers aftershocks (events 5~10 in Fig. 1b) occurring within the rupture zone at different depths and distances (plotted for each event), using model parameters given in Fig. 1b, fit to observed trapped waves (red lines) quite well. A double-couple source is located in the fault-zone waveguide. Both synthetic and observed seismograms have been low pass (<5 Hz) filtered and are plotted using a fixed scale in each plot

图 1 (a)对于发生在不同深度和震源距的 7 个兰德斯余震(见图 1b 中地震序号)和 3 个爆炸震源，作多带通滤波后测出的断层导向波群速度，显示断裂带内与深度相关的速度构造；(b)横跨 JVF 的破裂带结构模型的深度剖面；(c)使用三维有限差分方法和图 1b 中模型参数计算的合成地震波形(绿线)与测线 1 记录到的 6 个兰德斯余震(参见图 1b 中地震序号)产生的地震波(红线)相对照图

1994a, b].

From the view point of fracture mechanics, the fault-zone trapped wave inferred low-velocity waveguide on the Landers rupture zone represents the process zone (break-down zone) in crustal rock, in which inelastic deformation occurred around the propagating crack tip during dynamic rupture in the 1992 *M*7.1 mainshock although this distinct low-velocity zone could have accumulated the damage in fault-zone rock by historical earthquakes. Studies of repeated earthquakes along a fault [e. g. *Vidale et al.*, 1994] have shown that the ruptured fault zone could regain its strength following a large earthquake. This trend is consistent with state-and rate-dependent healing models [*Dieterich*, 1978; *Marone*, 1998]. Rupture models that involve variations in fault-zone fluid pressure over the earthquake cycle have also been proposed [*Sibson*, 1997; *Blanpied et al.*, 1998]. We probed the post-earthquake variation in fault strength and material properties of fault-zone rock by repeated seismic surveys using explosions at the Landers rupture zone from 1994 to 2001. These experiments revealed temporal changes in seismic velocity and rock rigidity of the JVF [*Li et al.*, 1998a, *Li and Vidale*, 2001, *Vidale and Li*, 2003].

Each experiment in repeated surveys was very similar: seismometers were re-buried in the same holes and the explosions, each shot using 300~500 kilograms of chemical explosives, were in 35 m shot-holes cosited with the previous years' holes within 10 m. Fig. 5a exhibits profiles on Line 1 across the JVF for explosion SP4 detonated within the rupture zone 5.7 km south of the array in 1994, 1996, 1998, 2000, and 2001. The waveforms of P, S, and trapped waves were similar in the repeated experiments. However, wave speeds varied with time. In order to measure the changes in travel time of these waves accurately, we extracted P, S and trapped waves from 3 time windows, respectively, and cross-correlated

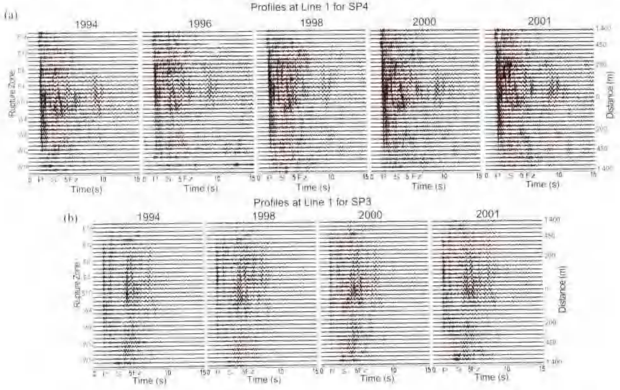

Fig. 5 (a) Vertical component seismograms recorded at Line 1 for shots SP4 detonated within the Landers rupture zone in repeated experiments in 1994, 1996, 1998, 2000, and 2001. The origin time of the shot is aligned at zero. Seismograms have been low pass (< 6 Hz) filtered and are plotted using a fixed scale in each plot. Seismograms recorded in repeated surveys show the similar waveforms. Two bars denote the width of rupture zone on the JVF, in which prominent fault-zone trapped waves were recorded. (b) As the same in (a), but for shot SP3 detonated in repeated experiments in 1994, 1998, 2000, and 2001

图5 (a)在1994,1996,1998,2000和2001年重复实验中由测线1记录到的爆炸震源SP4产生的垂直分量地震波形图,SP4位于兰德斯断裂带内,位于测线1南方约5 km处;(b)在1994,1998,2000和2001年重复实验中由测线1记录到的爆炸震源SP3产生的垂直分量地震波形图。SP3位于测线1北方约5 km处

each pair of recordings for the same shot and same seismometer to obtain traveltime differences between recordings in the repeated experiments. Fig. 6a, for example, shows seismograms recorded at station ST0, and auto-and cross-correlation between recordings. The peaks of the cross-correlation are almost one, indicating waveform similarity between repeated experiments. Cross-correlations revealed that traveltimes of P, S, and trapped waves decreased by 26, 35, and 50 ms between 1994 and 1996 and further decreased by 15, 25, and 35 ms between 1996 and 1998, but increased by 7, 12, and 16 ms between 1998 and 2000. The latest experiment in 2001 showed that traveltimes for P, S, and trapped waves decreased again by 7, 11, and 20 ms between 2000 and 2001. For another example, Fig. 5b displays profiles at Line 1 for shot SP3 detonated within the Landers rupture zone 4.8 km north of the array in 1994, 1998, 2000, and 2001. Again, similar waveforms of P, S, and trapped waves were recorded in the repeated experiments. The waveform cross correlations between repeated recordings at station ST0 show that traveltimes of these waves advanced by several tens of milliseconds between 1994 and 1998 (Fig. 6b). It is noted that the traveltime advance increases progressively with longer traveltimes for P, S, and trapped waves. P waves arrived 40 ms earlier while S and trapped waves arrived 65 and 82 ms earlier. If the velocity were uniform through the crust that was sampled by these waves, the decrease in traveltime would be straightforward to interpret. In this example, the traveltime of the P wave was ~1.5 s, so the P wave velocity increased by 2.6% between 1994 and 1998. Similarly, traveltimes of the S and trapped waves were 3.1 s and 4.2 s, respectively, so the S and trapped wave velocities increased by ~2% between 1994 and 1998. However, the trend in velocity increase was interrupted after 1998. Waveform cross-correlations at ST0 show that wave velocities decreased by ~0.4% between 1998 and 2000, but they increased again by ~0.5% between 2000 and 2001.

In Fig. 7a, the 3-D finite-difference synthetic fault zone trapped waves at Line 1 for shot SP3 are compared with those observed in the repeated surveys in 1994 and 1998. The model parameters in Fig. 1b are used for simulation of trapped waves in 1994. The trapped waves in 1998 are then computed using the same model but with a velocity increase of 2% for fault zone rock and 0.5% for the wall rock. Overlapping synthetic seismograms for 1994 and 1998 show that trapped waves traveled faster in 1998 than in 1994, consistent with observations. For further comparison, the cross-correlation of synthetic trapped waves at station ST0 exhibits 80 ms advance in traveltime between 1994 and 1998, agreeable well with that measured from the recordings in repeated surveys in 1994 and 1998. It is also evident that the fault-zone structural model with physical properties of fault-zone rock given in Fig. 4b is applicable to the Landers rupture zone.

The decrease in travel time of P, S, and trapped waves measured from cross-correlations of seismograms at all stations of Line 1 and Line 3 for shots at SP3, SP4, and SP5 between 1994 and 1996, and 1996 and 1998 are summarized in Fig. 7b. In average, the traveltimes of shear and trapped waves within the rupture zone decreased by ~1.2% between 1994 and 1996, and decreased further by ~0.7% between 1996 and 1998. In contrast, smaller changes in traveltimes of these waves occurred in the surrounding rocks. Fig. 7c shows the shear velocity increases around the JVF determined from the measurements of traveltime decreases for all shot-receiver pairs between 1994 and 1998. The greater velocity increase within the rupture zone indicates that the fault has been healing (strengthening) by the rigidity increase of fault zone rock after the Landers earthquake, most likely due to the closure of cracks that opened during the 1992 mainshock. This process may be interpreted as reductive dilatancy in the rock [*Nur*, 1972].

The change in velocity due to the change in the density of cracks can be calculated using equations in which the elastic constants of fractured rock are functions of the crack density [*O'Connell and Budiansky*, 1974]. The apparent crack density is defined by $e = N(a^3)/V$, where a is the radius of the flat penny shaped crack and N is the number of cracks in a volume V. Assuming randomly oriented cracks to be partially water filled and Poisson's ratio to be 0.33. Using an average $v_P = 2.0$ km/s and $v_S = 1.0$ km/s for the fault-zone rock at shallow depth, which have been determined from explosion-exciting trapped waves, the calculations revealed that the apparent crack density within the Landers rupture zone decreased by 0.03 between 1994 and 1998, which caused ~4% increase in shear rigidity of the fault zone rock.

Fig. 7d shows cumulated velocity variations of P, S, and trapped waves measured from waveform cross-correlations of recordings at stations located within the rupture zone for shots SP3, SP4, and SP5 in the repeated experiments in 1994, 1996, 1997, 1998, 2000, and 2001. The annual changes in velocity with time have been calculated from these data. The average annual increase in velocity within the Lan

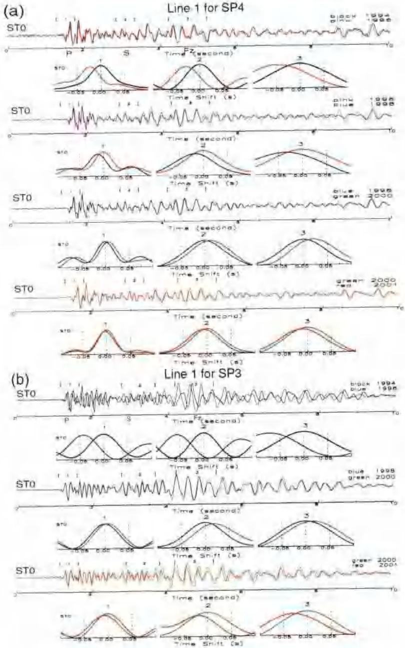

Fig. 6 (a) Vertical component seismograms recorded at station ST0 of Line 1 for shot SP4 in the repeated experiments are overlapped. Black line are auto-correlations of seismograms recorded in 1994, and ink lines are cross-correlations of recordings between 1994 and 1996 for 3 time windows [1] to [3] including P, S, and trapped waves, respectively. The peak of the auto-correlation curve is at zero lag time in each window. The negative time shift indicates time advance. The cross-correlations (pink lines) in windows [1] to [3] show time advances of 26, 35, and 50 ms for P, S, and trapped waves between 1994 and 1996. Similarly, the cross-correlations (blue lines) show that traveltimes for P, S, and further decreased by 15, 25, and 35 ms between 1996 and 1998. However, the cross-correlations (green lines) show that traveltimes increased by 7, 12, and 16 ms between 1998 and 2000. The cross-correlations (red lines) show that traveltimes decreased again by 7, 14, and 20 ms for P, S, and trapped waves between 2000 and 2001. (b) As the same in (a), but for shot SP3. The cross-correlations (blue lines) show time advances of 40, 65, and 82 ms for P, S, and trapped waves between 1994 and 1998. The cross-correlations (green lines) show that traveltimes retarded by 8, 13, and 18 ms for P, S, and trapped waves between 1998 and 2000. The cross-correlations (red lines) show time advances again by 10, 20, and 25 ms for P, S, and trapped waves between 2000 and 2001

图6 (a)在兰德斯断裂带进行的重复实验中由测线1上站台ST0记录到的爆炸震源SP4产生的垂直分量地震波形图和自相关及互相关曲线；(b)与(a)相同，只是换为爆炸震源SP3，显示重复记录到的地震波

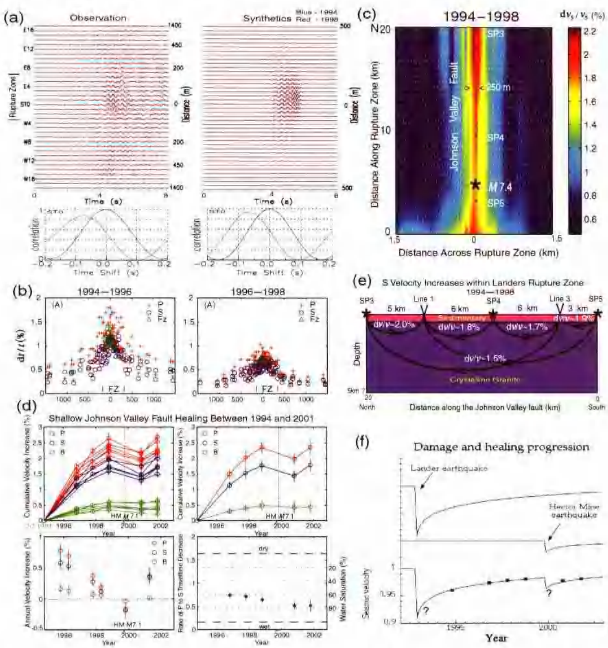

Fig. 7 (a) Observed and synthetic fault-zone guided waves at Line 1 for shot SP3 detonated within the Landers rupture zone in 1994 and 1998. Synthetic trapped waves are computed using the model in Fig. 3d for 1994 while velocities increase by 2% within the rupture zone and by 0.5% outside the rupture zone for 1998. Seismograms have been (<3 Hz) filtered. Autocorrelations (blue lines) and cross-correlations (red lines) for synthetic waveforms at station ST0 between 1994 and 1998 agreeable with observations. (b) Travel time decreases in percent for P, S and guided waves determined from cross-correlations of seismograms recorded at all stations of Lines 1 and 3 for shots SP4 and SP5 in repeated experiments. The greater decreases in traveltime occurred within the rupture zone. Traveltimes decreased more between 1994 and 1996 than between 1996 and 1998. (c) The map shows S velocity increases between 1994 and 1998 around the JVF, measured at Lines 1 and 3 for shots SP3, SP4 and SP5. Velocity increases are greater within the rupture zone and vary along the rupture zone. (d) Cumulated changes of P and S velocities for 6 shot-array pairs measured at the 5 stations closest to the surface fault trace within the Landers rupture zone between 1994 and 2001. 4 stations outside the fault zone, about 1 km on either side of the fault trace, shown by the green symbols, show less velocity change than stations within the rupture zone. The vertical dashed lines indicate the time of the Hector Mine earthquake. Repeated experiments were conducted in October of each year. The right top plot 20 shows average and standard deviation of cumulative velocity changes between 1994 and 2001 from combing the six shot-array paths. The left bottom panel shows the estimated annual increase and standard deviation in velocity with time. The right bottom panel shows the ratio of P to S travel time changes with time, which is sensitive to the degree of fluid saturation in cracks. Horizontal dashed lines show the ratios predicted for a range of water saturation percentages. (e) Depth section on the JVF shows the depth-dependent S velocity increases measured within the Landers rupture zone. Approximate depth of seismic ray penetration and inferred accumulated healing at each depth. (f) Model of velocity as a function of time due to damage from the Landers rupture, the Hector Mine shaking, and the sum of the two compared with observations. Healing as the logarithm of time is shown, although details just after each event and extrapolating into the future are not well constrained. The velocity before the Landers earthquake was not measured

图 7　(a)1994 年和 1998 年在兰德斯测线 1 上观察到的由震源 SP3 产生的地震波和三维有限差分拟合的断层导向波相对照；显示波震波、波速在 1998 年比 1994 年快；(b)在 1994、1996 和 1998 年重复实验中测线 1 和 3 上所有站台记录到的震源 SP4 和 SP5 产生的地震波经相关波形计算得出的 P 波、S 波和断层导向波传播时间递减的百分比；(c)显示 1994 年和 1998 年间在兰德斯断裂带沿 JVF 测出的 S 波波速增加分布图；数据来自测线 1 和 3 及震源 SP3、SP4 和 SP5；(d)1994 年和 2001 年间在兰德斯断裂带内最靠近断层的 5 个站台上测定的 P 波和 S 波波速随时间累结变化；(e)沿 JVF 的深度剖面；显示在兰德斯断裂带内测定的 S 波波速增加与深度有关；(f)兰德斯和海克特曼恩断裂带内波速随时间变化的模型和观察结果对照图

ders rupture zone was ~0.8% for P waves and ~0.6% for S and trapped waves in the early stage, but became smaller to ~0.3% and ~0.2% in the late stage between 1994 and 1998, indicating that the healing rate is not constant but decreasing with time. However, P and S velocities decreased by ~0.4% between 1998 and 2000, and then increased again by about ~0.5% from 2000 to 2001. The decrease in velocity between 1998 and 2000 might be caused by the *M*7.1 Hector Mine earthquake occurring ~25 km east of the Landers rupture zone. The Hector Mine earthquake could have caused the observed change in seismic wave speed in two ways. These involve dynamic and static stresses, which have already been cited as possible mechanisms for triggering distant aftershocks and inducing deformation on faults. Dynamic stresses during the Hector Mine earthquake on the JVF were a few MPa while static stress changes due to the earthquake are perhaps half an MPa [*Fialko et al.*, 2002]. Thus, most probably, the dynamic stresses during the strong shaking cracked connections in the rock, as we infer the Landers mainshock did in 1992, but to a lesser degree. This damage is healing in subsequent years, just as we observe the main shock damage to be healing. The conceptual model is illustrated in Fig. 7f [*Vidale and Li*, 2003]. Alternatively, the static stress change doesn't work as well as the shaking from dynamic waves although it remains viable. The strain observed around the faults was a step-function in time, but the velocity changes were more protracted. However, the observation of strain concentrated on fault zones [*Fialko et al.*, 2002] is consistent with our interpretation of dynamic shaking as the cause of the rock damage, because concentrated deformation may help cause damage of compliant rock, and low-strength fault zones are sensitive to damage due to their fractured nature and the wave amplification caused by their low impedance.

The calculated ratio of changes in traveltimes for P to S waves ($\Delta t_P/\Delta t_S$) decreased from 0.75 to 0.55 between 1994 and 2001 (Fig. 7c) indicates that cracks within the rupture zone were partially water saturated and became more wet with time [*Li and Vidale*, 2001]. From this evidence, it appears that some partially saturated crustal cracks, which had opened during the mainshock, closed soon thereafter. Closure of cracks increases the frictional strength of the fault zone, as well as rock stiffness. This is consistent with the tentative interpretation of the well-developed low-velocity Landers fault-zone waveguide as being at least partially created during the mainshock, although it likely also represents a worn zone that has accumulated over geologic time.

The depth dependence of the inferred healing is illustrated in Fig. 7d. It also shows that the healing rate was greater near the stepover between the JVF and HVF at shallow depth probably related to the stress controlled fluid redistribution around the fault stepover [*Peltzer et al.*, 1998]. It is known that structural and rheological fault variations, as well as spatial and temporal variations in strength and stress, will affect the earthquake rupture [e.g., *Wesson and Ellsworth*, 1973; *Das and Aki*, 1977; *Rice*, 1980; *Vidale et al.*, 1994; *Beroza, et al.*, 1995]. Study of the internal structure in 4-D at the Landers rupture zone holds the key to understanding the physics of earthquakes.

2　At the Hector Mine Rupture Zone

The Hector Mine earthquake on October 16, 1999, is the second *M*7+ quake with surface exposure in southern California in the past decades. It provides another appropriate site for a fault zone trapped wave study. The $M7.1$ Hector Mine earthquake occurred in the eastern California shear zone, only 25 km northeast of the epicenter of the 1992 $M7.5$ Landers earthquake, and produced a 40 km-long surface rupture involving portions of multiple fault zones (Fig. 1a). This pattern of rupture along more than one mapped fault is similar to that from the Landers earthquake, but more complicated at the depth than surface breaks. On the Lavic Lake fault (LLF) in the Bullion Mountains, the faulting with the maximum rightlateral strike slip of 5 m is relatively simple with most of slip on a single trace, or closely spaced parallel traces within the width range of tens of meters. This pattern is in contrast to the complex faulting pattern with bifurcation in the northern and southern portions of the rupture zone.

The complex multiple-faulting pattern of the Hector Mine rupture zone at seismogenic depths has been investigated using fault-zone trapped waves generated by near-surface explosions and aftershocks, and recorded at linear seismic arrays deployed across the surface rupture [*Li et al.*, 2002, 2003a]. Immediately after the mainshock, a Geometrics Strata View exploration Seismograph with 20 three-component sensors were deployed on a tight seismic line across the north LLF in Bullion Mountains [*Li*, 2000]. 4~7 Hz faultzone trapped waves were recorded for aftershocks occurring within the rupture zone. These trapped waves are similar to those observed at the Landers rupture zone but show higher frequencies, implying a narrower low-velocity waveguide on the Hector Mine rupture zone. For a more detailed delineation of slip planes at depth, 3 linear seismic arrays of 60 three-component REFTEK seismometers were deployed across the LLF and the Bullion Fault (BF) to record fault-zone trapped waves generated by aftershocks and explosions detonated within the rupture zone. Locations of seismic arrays, explosions, and aftershocks recorded during the experiment are shown in Fig. 1c. Array 1 was composed of 16 three-component stations along a 350 m long line across the north LLF in the Bullion Mountains. Array 2 and Array 3 were each 500 m long and composed of 20 stations. These two arrays were located 18 km south of the mainshock epicenter and ~1 km apart from each other. Station spacing in the arrays was not even, with 12.5 m separation for stations close to the main fault trace, and 25 or 50 m spacing for farther stations. Station ST0, at the center of each array, was deployed on the main fault trace. The LLF experienced 4 m right-lateral slip at site Array 1, which was ~6 km south of the 1999 $M7.1$ Hector Mine earthquake epicenter. The rupture zone at the surface is ~75 m wide, including one major and several minor parallel faults with the mainshock slip. The lateral slips were ~1 m at site Array 3 across the south LLF, and 0.5 m at Array 2 across the southeast BF. The rupture extended 10 km further along the south LLF while slip diminished quickly to the south on the southeast BF. The recurrence interval of faulting on the LLF and BF is thousands of years.

Fig. 8a shows three-component seismograms recorded at Array 1 across the north LLF for 2 $M1.7$ aftershocks (events 7 and 11 in Fig. 1c) occurring at the depth of 4.5 km and 9 km from the array. Prominent fault-zone guided (trapped) waves with large amplitudes and long duration after S waves were recorded at stations between E3 and W3 close to the LLF main fault trace for event 7 located within the rupture zone, but not for event 11 occurring ~5 km away from the rupture zone. Stations out of the rupture zone registered brief wavetrains of P and S waves for both events. The duration of trapped wavetrains after S waves in three components are not the same, probably due to the anisotropy of fault-zone rock. Fig. 8b exhibits seismograms at Array 1 for other three M~1.5 aftershocks (events 3, 13, and 23 in Fig. 1c) occurring at depths of 3, 7.6, and 11.7 km within the rupture zone near Array 1. Again, significant trapped waves appeared at stations close to the fault trace. The duration of trapped waves after S waves increases with hypocentral distance of the event, showing a continuous low-velocity waveguide on the LLF to seismogenic depth. It is noted that the separation time between S and dominant trapped waves is not linearly proportional to the depth, indicating the less velocity reduction within the narrower waveguide at deeper level of the rupture zone. The multiple band-pass filtered seismograms at station ST0 in 9 frequency bands between 3.3 and 7.5 Hz and their envelopes for these events show the dispersion of trapped waves with the slower speed at higher frequencies. In contrast, there is no dispersion with S waves. The group velocities of trapped waves have been derived from band-pass filtered seismograms. They range from ~2.5 km/s at 3.3 Hz to ~1.8 km/s at 6 Hz for event 23, from 3 km/s at 3.3 Hz to 2.0 km/s at 6 Hz for event 13, and from 3.3 km/s at 3.3 Hz to 2.4 km/s at 6 Hz for event 3. The measured group velocities show a depthdependent velocity structure within the Hector Mine rupture zone similar to the Landers rupture zone.

A systematic waveform analysis for aftershocks occurring in the northern Hector Mine epicentral area revealed two groups of aftershocks that generated prominent fault-zone trapped waves. Aftershocks in the first group occurred on the north LLF which broke to the surface in the 1999 $M7.1$ mainshock. Af-

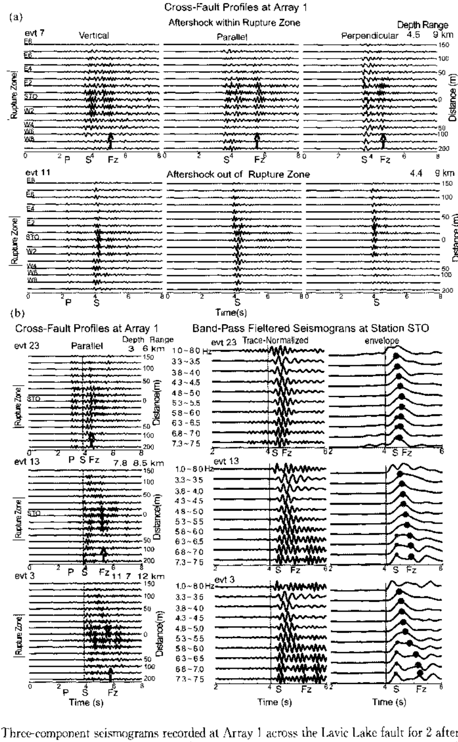

Fig. 8 (a) Three-component seismograms recorded at Array 1 across the Lavic Lake fault for 2 aftershocks (events 7, and 11 in Fig. 1c), occurring within and ~3 km away from the Hector Mine rupture, respectively. Station ST0 was located at the main fault trace. The distances of other stations from the fault trace are plotted at right to profiles. The depth and hypocentral distance (range in km) of the events are shown at the upper right of each plot. Seismograms have been low-pass (< 7 Hz) filtered and are plotted using a fixed amplitude scale in each profile. Prominent fault-zone guided waves (Fz) were recorded for event 7 but not for event 11 although they had almost the same depths and distances from the array. Solid bars mark the rupture zone width inferred by trapped waves, within which one major and several minor faults were seen at this site. Other notations are the same as in Fig. 2. (b) Left: Fault-parallel component seismograms at Array 1 for 3 aftershocks (events 3, 13, and 23 in Fig. 1c) occurring within the rupture zone at the same location but different depths. Vertical dashed lines align with the S arrivals. Arrows denote the dominant guided waves. The separation between S and guided wave arrivals increases with the distance between the event and array. Middle: Parallel-fault component seismograms at station ST0 of Array 1 for events 3, 5, and 13 are filtered in 9 frequency bands between 3.3 and 7.5 Hz. Multiple band-pass filtered seismograms are plotted in the trace-normalized profile. Right: Computed envelopes of filtered seismograms. The peak of envelope marked by a circle denotes the arrival of fault-zone trapped energy at the specified frequency band, showing dispersion of guided waves. Small circles denote the amplitudes of S waves, showing without dispersion

图 8 (a)在横跨 Lavic Lake(LLF)断层的地震台阵 1 记录到的由 2 个海克特曼恩余震(图 1c 中地震序号 7 和 11)产生的 3 分量地震波形图;两余震分别发生在断裂内和距断裂带 3 公里;(b)左图:在台阵 1 上记录到的由 3 个海克特曼恩余震(图 1c 中地震序号 3,13 及 23)产生的平行断层分量上的地震波形;3 个余震发生在相同地点但震深不同;中图:在台阵 1 上站台 ST0 记录的余震波形经过 3.3 到 7.5Hz 之间 9 个频带滤波;右图:经滤波后计算取得的振幅包络显示断层导向波的频散特征

tershocks in the second group were located along a buried unknown fault with more northerly direction from the mainshock epicenter (Fig. 1c). In contrast, aftershocks occurring elsewhere did not generate significant fault-zone guided waves. Fig. 9a exhibits seismograms recorded at Array 1 for 3 aftershocks (events 16, 4, and 9 in Fig. 1c) located at ~15 km north of the array. Fault-zone trapped waves with large amplitudes and long duration after S waves appeared at stations within the rupture zone for events 16 and 4 occurring on the north LLF and the buried fault, respectively, but not for event 9 occurring between them. Fig. 9b shows further examples of fault zone trapped waves recorded at Array 1 for 6 aftershocks (events 1, 2, 5, 17, 19, and 21 in Fig. 1c) occurring along the north LLF and buried fault at different distances. The separation between arrival times of S and dominant trapped waves increases with the hypocentral distance of these events, showing the existence of low-velocity waveguides on the north LLF and also on a buried fault. Since trapped waves generated by the events on the north LLF and the buried fault showed similar features, we interpret that this buried fault ruptured at depth in the 1999 earthquake although it did not break to the surface.

Fault zone trapped waves were also successfully generated by explosions detonated at the Hector Mine rupture zone. Fig. 10a exhibits prominent guided waves recorded at Array 1 for explosion SP2 located at the middle LLF, 7.5 km south of the array (Fig. 1c). Trapped waves appeared at stations within the rupture zone between 4.5 and 6 s but continue until 9 s, showing multiple trapped wavetrains. The coda normalized amplitude spectra of trapped waves for a 3 s time window starting from the S arrivals show a maximum at about 3~4 Hz at stations within the rupture zone, which decreases with station offset from the fault trace. The dominant frequency of explosion-exciting trapped waves is lower than those generated by aftershocks, indicating that the rupture zone is wider and softer at the shallow depth. Explosion-exciting fault-zone trapped waves show dispersion in the multiple band-pass filtered seismograms at 5 frequency bands: 1.0~8.0 Hz, 1.8~2.0 Hz, 2.8~3.0 Hz, 3.8~4.0 Hz, and 4.8~5.0 Hz. Trapped waves at higher frequencies travel more slowly but more concentrated within the rupture zone than those at lower frequencies. The lower frequency energy is apt to penetrate into the wall-rocks. Fig. 10b shows the clearer dispersion of guided waves in multiple band-pass filtered seismograms in 9 frequency bands between 1.8 and 6.0 Hz at station ST0. The peak of computed envelope of filtered seismograms using a Hilbert transformation in the envelope indicates the arrival of energy in the specified frequency band. Trapped waves at 3~4 Hz are dominant in the true-amplitude profile. Again, we see that trapped waves at higher frequencies travel slower than those at lower frequencies. In contrast, S waves are lack of dispersion. From multiple band-pass filtered seismograms registered at stations located within the rupture zone for shot SP2, the measured group velocities of fault-zone guided waves range from ~1.7 km/s at 1.8 Hz to ~1.3 km/s at 6 Hz. Group velocities of guided waves were also measured for other shots and arrays, and used as constraints for the shallow fault zone structure in modeling.

In order to minimize the source and site affects on trapped wave analysis, amplitude spectral ratios of trapped waves to P waves have been computed. For example, Fig. 11a exhibits the amplitude ratios of trapped waves to P waves for 10 Hector Mine aftershocks. For events within the rupture zone, the ratios show a maximum peak at 4~6 Hz at stations close to the fault trace, which decreases rapidly with the distance from the fault trace. In contrast, the ratios for events occurring away from the rupture zone are nearly the same at all stations because these events did not generate significant fault-zone trapped waves. The pattern of spectral ratios allow us to determine which aftershocks occurred within or out of the rupture zone so that they are helpful for a delineation of fault zone branches.

The bifurcation of the northern Hector Mine rupture zone at depth delineated by trapped waves is in accord with the complex pattern of aftershock distribution [*Hauksson et al.*, 2002], and the rupture model of inversion of ground motion, telemetry, geodetic data and surface breaks [*Ji et al.*, 2002]. The